Electronic Supplementary Information (ESI) for

Dalton Transactions

Regulation of magnetic relaxation behavior by replacing of 3d transition metal ions for the $[M_2Dy_2]$ complexes containing two kinds of organic chelating ligands

Hui-Sheng Wang,[*a] Cheng-Ling Yin,[a] Zhao-Bo Hu,[b] Yong Chen,[a] Zhi-Quan Pan,[a] You Song,[*b] Yi-Quan Zhang,[*c] and Zai-Chao Zhang [d]

[a] School of Chemistry and Environmental Engineering, Key Laboratory of Green Chemical Process of Ministry of Education, Wuhan Institute of Technology, Wuhan 430074, P. R. China.

[b] State Key Laboratory of Coordination Chemistry, School of Chemistry and Chemical Engineering, Collaborative Innovation Center of Advanced Microstructures, Nanjing University, Nanjing 210046, P. R. China.

[c] Jiangsu Key Laboratory for NSLSCS, School of Physical Science and Technology, Nanjing Normal University, Nanjing 210023, China.

[d] Jiangsu Key Laboratory for the Chemistry of Low-dimensional Materials, School of Chemistry and Chemical Engineering, Huaiyin Normal University, P. R. China.

Corresponding author, E-mail: wangch198201@163.com, Fax: +86-27-87194560 (H.-S Wang); yousong@nju.edu.cn (Y. Song) and E-mail: zhangyiquan@njnu.edu.cn (Y.-Q. Zhang)

Contents

Table S1. Crystal data and structure refinement parameters for **1**, **1'**, **2** and **2'**.

Compounds	**1**	**1'**	**2**	**2'**
Formula [*]	$C_{60}H_{84}Cl_2Dy_2Fe_2N_{14}O_{20}$	$C_{60}H_{84}Cl_2Fe_2Gd_2N_{14}O_{20}$	$C_{65}H_{99}Co_2Dy_2N_{10}O_{31.50}$	$C_{66}H_{101}Co_2Gd_2N_{10}O_{31.50}$
Formula weight [*]	1829.01	1818.51	1967.40	1970.92
Temperature	173(2)	173(2)	173(2)	173(2)
Wavelength (Å)	0.71073	0.71073	0.71073	0.71073
Crystal system	Monoclinic	Monoclinic	Triclinic	Triclinic
Space group	$P2_1/n$	$P2_1/n$	$P\bar{1}$	$P\bar{1}$
a (Å)	11.4988(7)	11.5322(5)	9.8087(4)	9.8667(6)
b [Å]	9.7823(6)	9.6271(4)	13.3481(6)	13.3781(8)
c [Å]	30.8793(19)	32.6696(12)	14.8569(7)	14.8804(8)
α [°]	90	90	85.486(2)	85.483(2)
β [°]	94.418(2)	94.5820(10)	87.309(2)	87.541(2)
γ [°]	90	90	82.961(2)	82.719(2)
V [Å^3]	3463.1(4)	3615.4(3)	1923.16(15)	1941.2(2)
Z	2	2	1	1
D_c [g/cm^{-3}]	1.754	1.670	1.699	1.686
μ (Mo Kα) [mm^{-1}]	2.703	2.357	2.436	2.198
F(000)	1840	1832	997	1001
Crystal size (mm)	0.22 × 0.12 × 0.08	0.24 × 0.18 × 0.07	0.18 × 0.11× 0.07	0.36 × 0.22× 0.17
θ range (°)	2.8768~25.1586	2.9713~25.3156	3.0547~26.1746	3.0441~25.3101
Index ranges	−13 ≤ h ≤ 13 −11 ≤ k ≤ 11 −36 ≤ l ≤ 36	−13 ≤ h ≤ 13 −11 ≤ k ≤ 10 −38 ≤ l ≤ 38	−10 ≤ h ≤ 11 −15 ≤ k ≤ 15 −17 ≤ l ≤ 17	−10 ≤ h ≤ 11 −15 ≤ k ≤ 15 −17 ≤ l ≤ 17
Reflections collected	34607	23872	28458	14692
Unique reflections [R_{int}]	6074 [0.0651]	6306 [0.0554]	6755 [0.0760]	6783 [0.0749]
Reflections with $I > 2\sigma(I)$	4799	5102	5294	5337
Goodness-of-fit on F^2	1.176	1.083	1.032	1.088
Final R indices [I>2sigma(I)]	R_1[a] =0.0912, wR_2[b] = 0.1855	R_1[a] =0.0569, wR_2[b] = 0.1033	R_1[a] = 0.0382, wR_2[b] =0.0564	R_1[a] = 0.0420, wR_2[b] =0.0650
R indices (all data)	R_1 =0.1170, wR_2 = 0.1927	R_1 =0.0800, wR_2 = 0.1087	R_1 = 0.0636, wR_2 = 0.0598	R_1 = 0.0658, wR_2 = 0.0688
S (all data)	1.182	1.084	1.033	1.089
$(\Delta\rho)_{max,min}$/e Å^{-3}	6.037 and -5.801	1.011 and -1.387	0.823 and -0.609	1.750 and -0.988

[*] the formula and formula weight include the solvent molecules in the crystal lattices, which were subtracted by the SQUEEZE program. [a] $R_1 = \Sigma(||F_o| - |F_c||)/\Sigma|F_o|$. [b] $wR_2 = [\Sigma[w(F_o^2 - F_c^2)^2]/\Sigma[w(F_o^2)^2]]^{1/2}$, $w = 1/[\sigma^2(F_o^2)\ (ap)^2 + bp]$, where $p = [\max(F_o^2, 0) + 2F_c^2]/3$.

Table S2. Selected bond lengths (Å) and angles (°) for complexes **1** and **1'**.

Selected bond lengths for **1**					
Cl1-Dy1	2.691(3)	Dy1-O6	2.467(10)	Fe1-O2	2.025(9)
Dy1-O7	2.239(9)	Dy1-N4	2.558(11)	Fe1-N3	2.099(12)
Dy1-O5	2.302(9)	Fe1-O5	1.924(9)	Fe1-N1	2.128(12)
Dy1-O2	2.379(9)	Fe1-O1	1.934(9)	Fe1-N2	2.220(11)
Selected bond lengths for **1'**					
Cl1-Gd1	2.7382(18)	Gd1-O6	2.483(5）	Fe1-O2	2.036(5)
Gd1-O7	2.271(5)	Gd1-N4	2.583(6)	Fe1-N3	2.106(7)
Gd1-O5	2.333(5)	Fe1-O1	1.929(5)	Fe1-N1	2.132(6)
Gd1-O2	2.425(5)	Fe1-O5	1.951(5)	Fe1-N2	2.227(7)
Selected bond angles for **1**					
O7-Dy1-O7	71.2(3)	O6-Dy1-Cl1	90.4(2)	O2-Fe2-N3	83.9(4)
O7-Dy1-O5	101.4(3)	N4-Dy1-Cl1	83.1(2)	O5-Fe2-N1	100.7(4)
O7-Dy1-O5^{i}	83.1(3)	O6-Dy1-N4	66.2(3)	O2-Fe2-N2	109.8(3)
O7-Dy1-O2	82.0(3)	O7-Dy1-O6	153.5(3)	N3-Fe2-N2	77.7(4)
O7-Dy1-O2^{i}	133.2(3)	O7-Dy1-O6^{i}	135.1(3)	O5-Fe2-O1	100.1(4)
O5-Dy1-O2	65.0(3)	O5-Dy1-O6	82.7(3)	O5-Fe2-O2	78.9(3)
O7-Dy1-Cl1	96.4(2)	O2-Dy1-N4	123.9(3)	O1-Fe2-O2	87.6(3)
O7-Dy1-Cl1^{i}	83.5(2)	O1-Fe2-N3	99.5(4)	O5-Fe2-N3	153.2(4)
Selected bond angles for **1'**					
O7-Gd1-O7^{ii}	70.2(2) .	O2-Gd1-O6	81.50(17)	O5-Fe1-N3	152.7(2)
O7-Gd1-O5	103.75(18)	O7-Gd1-N4	138.48(18)	O2-Fe1-N3	82.9(2)
O7-Gd1-O5^{ii}	83.32(17)	O7-Gd1-N4^{ii}	68.37(18)	O1-Fe1-N1	86.1(2)
O7-Gd1-O2	80.99(16)	O6-Gd1-Cl1	88.69(13)	O5-Fe1-N1	101.9(2)
O7-Gd1-O2^{ii}	130.65(16)	N4-Gd1-Cl1	83.81(15)	O2-Fe1-N1	172.1(2)
O5-Gd1-O2	65.38(16)	O6-Gd1-N4	65.61(18)	N3-Fe1-N1	97.7(3)
O7-Gd1-O6	155.91(18)	O7-Gd1-O4	90.65(17)	O1-Fe1-N2	162.6(2)
O5-Gd1-O6	83.67(17)	O1-Fe1-N3	101.5(3)	O5-Fe1-N2	89.6(2)

Symmetry code: ^{i} 1-x, 1-y, -z; ^{ii} –x, 2-y, 1-z.

Table S3. Selected bond lengths (Å) and angles (°) for complexes **2** and **2'**.

Selected bond lengths for **2**					
Co1-N3	1.891(6)	Co1-Dy1	3.4899(9)	Dy1-O8	2.427(4)
Co1-O5	1.895(4)	Dy1-O6	2.258(4)	Dy1-O1	2.479(4)
Co1-N1	1.903(6)	Dy1-O6	2.343(4)	Dy1-N4	2.489(5)
Co1-O1	1.951(4)	Dy1-O7	2.362(4)	Dy1-O9	2.501(4)
Co1-N2	1.963(6)	Dy1-O5	2.384(4)	Dy1-O3	2.717(4)
Selected bond lengths for **2'**					
Co1-N1	1.892(6)	Gd1-O6	2.365(4)	Co1-N2	1.965(6)
Co1-O1	1.896(4)	Gd1-O7	2.394(4)	Co1-Gd1	3.5125(9)
Co1-O5	1.899(4)	Gd1-O5	2.424(4)	Gd1-O6	2.305(4)
Co1-N3	1.910(5)	Gd1-O8	2.460(4)	Gd1-N4	2.527(5)
Co1-O2	1.954(4)	Gd1-O2	2.496(4)	Gd1-O9	2.528(4)
Selected bond angles for **2**					
O2-Co1-N3	92.4(2)	O6-Dy1-O5^{iii}	143.82(14)	O6-Dy1-N4	64.50(15)
O2-Co1-O5	89.84(19)	O6-Dy1-O5	117.10(14)	O7-Dy1-N4	87.20(16)
O2-Co1-N1	97.7(2)	O7-Dy1-O5	134.26(14)	O1-Dy1-O9	75.59(14)
O2-Co1-O1	86.10(19)	O6-Dy1-O8^{iii}	73.70(15)	N4-Dy1-O9	80.12(16)
O1-Co1-N2	97.5(2)	O6-Dy1-O8	77.51(14)	O6-Dy1-O3^{iii}	67.50(13)
O6-Dy1-O6	73.94(15)	O5-Dy1-O1	63.77(14)	O6-Dy1-O3	128.35(13)
O6-Dy1-O7^{iii}	81.49(14)	O8-Dy1-O1	77.10(14)	O1-Dy1-O3	60.66(13)
O6-Dy1-O7	71.96(14)	O6-Dy1-N4^{iii}	138.41(15)	N4-Dy1-O3	143.33(15)
Selected bond angles for **2'**					
N1-Co1-O1	92.2(2)	O6-Gd1-O5	143.90(13)	O6 Gd1 N4	138.24(12)
N1-Co1-O5	95.8(2)	O6-Gd1-O5^{iv}	115.89(14)	O6 Gd1 N4^{iv}	63.77(11)
O1-Co1-O5	90.25(18)	O6-Gd1-O8	77.97(14)	O7 Gd1 N4	87.55(11)
N1-Co1-N3	91.6(2)	O7-Gd1-O8	144.69(15)	O5 Gd1 N4	62.21(11)
O1-Co1-N3	97.3(2)	O5-Gd1-O8	75.64(14)	O8 Gd1 N4	95.45(11)
O5-Co1-N3	169.1(2)	O6-Gd1-O2	91.52(13)	O2 Gd1 N4	125.28(12)
N1-Co1-O2	178.3(2)	O6-Gd1-O2	153.45(13)	O9 Gd1 N4	80.05(11)
O1-Co1-O2	86.08(18)	O2 Gd1 O9	75.64(10)	O6 Gd1 O4	67.83(10)

Symmetry code: ^{iii} -x, 1-y, 1-z; ^{iv} –x, -y, 2-z.

Table S4. Bond Valence Sum calculations for determining of the oxidation of the Fe and Co atoms in **1** and **2**.[a]

Fe atom in complex **1**	Fe(II)	Fe(III)
Fe(1)	2.5	<u>2.99</u>
Co atom in complex **2**	Co(II)	Co(III)
Co(1)	4.0	<u>3.5</u>

[a]The underlined value is the closest to the charge for which it was calculated. The oxidation state is the nearest whole number to the underlined value.

Table S5. Bond Valence Sum calculations for determining of the protonation levels of the O atoms from the ligands in **1** and **2**.

Atoms in **1**	BVS values of **1**	Atoms in **2**	BVS values of in **2**
O1	1.80	O1	1.97
O2	1.99	O2	1.82
O4	2.01	O3	2.08
O5	2.04	O5	2.02
O6	1.19	O6	1.95
O7	1.93	O7	1.88
		O8	1.8
		O9	1.12

The values of BVS calculations for O atoms in the ~1.8–2.0, ~1.0–1.2, and ~0.2–0.4 ranges are indicative of non-, single- and double-protonation, respectively

Table S6. The possible geometries of oct-coordination metal centers and Deviation parameters from each ideal polyhedron for Dy of complex **1**.

Point group	Geometry	Polyhedron	Dy1
D_{8h}	OP-8	Octagon	32.171
C_{7v}	HPY-8	Heptagonal pyramid	24.643
D_{6h}	HBPY-8	Hexagonal bipyramid	13.547
O_h	CU-8	Cube	12.342
D_{4d}	SAPR-8	Square antiprism	3.89
D_{2d}	TDD-8	Triangular dodecahedron	2.078
D_{2d}	JGBF-8	Johnson - Gyrobifastigium (J26)	10.348
D_{3h}	JETBPY-8	Johnson - Elongated triangular bipyramid (J14)	27.737
C_{2v}	JBTP-8	Johnson - Biaugmented trigonal prism (J50)	3.469
C_{2v}	BTPR-8	Biaugmented trigonal prism	3.303
D_{2d}	JSD-8	Snub disphenoid (J84)	3.426
T_d	TT-8	Triakis tetrahedron	13.124
D_{3h}	ETBPY-8	Elongated trigonal bipyramid	24.312

Table S7. The possible geometries of nona-coordination metal centers and Deviation parameters from each ideal polyhedron for Dy of complex **2**.

Point group	Geometry	Polyhedron	Dy1
D_{9h}	EP-9	Enneagon	32.969
C_{8v}	OPY-9	Octagonal pyramid	22.277
D_{7h}	HBPY-9	Heptagonal bipyramid	16.59
C_{3v}	JTC-9	Triangular cupola (J3) = trivacant cuboctahedron	15.29
C_{4v}	JCCU-9	Capped cube (Elongated square pyramid, J8)	9.588
C_{4v}	6CCU-9	Capped cube	7.996
C_{4v}	JCSAPR-9	Capped sq. antiprism (Gyroelongated square pyramid J10)	1.953
C_{4v}	CSAPR-9	Capped square antiprism	1.565
D_{3h}	JTCTPR-9	Tricapped trigonal prism (J51)	2.667
D_{3h}	TCTPR-9	Tricapped trigonal prism	2.093
C_{3v}	JTDIC-9	Tridiminished icosahedron (J63)	13.086
C_{2v}	HH-9	Hula-hoop	8.122
C_s	MFF-9	Muffin C	1.454

Table S8. E_a and τ_0 values obtained by fitting the data of $\ln(\chi''/\chi')$ *versus* $1/T$ at different frequencies for **1**.[a]

Frequency	E_a	τ_0	Frequency	E_a	τ_0
115 Hz	6.23 K	4.5×10^{-7}	370 Hz	7.57 K	2.2×10^{-7}
184 Hz	6.53 K	2.9×10^{-7}	1488 Hz	7.13 K	8.0×10^{-8}

[a] The mean values of E_a and τ_0 are 6.9 K and 2.6×10^{-7}, respectively.

Table S9. Satisfied parameters obtained for the extended Debye model with ac susceptibility data from SQUID magnetometer of compound **2** in the zero applied field.

	T(K)	χ_S	χ_T	τ (s)	α	Residual
1	1.80011	0.14233	0.55004	0.0077	0.15769	0.001620
2	1.99968	0.12877	0.57722	0.00769	0.1433	0.001330
3	2.4998	0.1086	0.61386	0.00729	0.10782	0.000899
4	2.99958	0.09154	0.63013	0.00695	0.10358	0.000880
5	3.50001	0.08225	0.62543	0.00652	0.09416	0.000766
6	3.99996	0.07452	0.61307	0.0061	0.09341	0.000518
7	4.49998	0.06847	0.59302	0.00561	0.09106	0.000394
8	5.0005	0.06199	0.57471	0.0051	0.09651	0.000551

9	5.49996	0.05834	0.53644	0.00435	0.08082	0.007240
10	6.00052	0.05461	0.52729	0.00387	0.09266	0.000345
11	7.00011	0.04741	0.48681	0.00273	0.09776	0.000309
12	7.99984	0.04254	0.4478	0.00181	0.0977	0.000232
13	8.99979	0.03842	0.41367	0.00117	0.09911	0.000242
14	10.00038	0.03613	0.38445	7.46E-04	0.10516	0.000179
15	11.00001	0.03596	0.3581	4.72E-04	0.114	0.000206
16	11.50093	0.03946	0.34702	3.83E-04	0.11658	0.000148
17	11.9999	0.04678	0.33455	3.09E-04	0.1147	0.000276
18	12.49989	0.04983	0.32508	2.43E-04	0.12859	0.000236
19	12.99995	0.05397	0.31425	1.90E-04	0.13276	0.000325

Table S10. Satisfied parameters obtained for the extended Debye model with ac susceptibility data from SQUID magnetometer of compound **2** in the 2000 Oe applied field.

	T(K)	χ_S	χ_T	τ (s)	α	Residual
1	1.80041	0.04893	0.699	0.04437	0.33054	0.00968
2	2.00016	0.04343	0.74949	0.04472	0.34767	0.00314
3	2.49988	0.03614	0.72079	0.02711	0.33993	0.00387
4	2.99994	0.03851	0.70702	0.02419	0.32807	0.00752
5	3.49994	0.03704	0.6767	0.0173	0.30279	0.00392
6	4.00007	0.03073	0.67313	0.01582	0.31831	0.00172
7	4.50005	0.03325	0.65253	0.01344	0.29521	0.00563
8	5.00005	0.03057	0.61662	0.00959	0.27213	0.00295
9	5.50017	0.03185	0.55346	0.00669	0.22958	0.00583
10	5.99997	0.02865	0.53767	0.00546	0.22557	0.00138
11	7.00004	0.02015	0.489	0.00341	0.2175	0.00174
12	8.00541	0.0316	0.45035	0.00191	0.13104	0.00274
13	9.00000	0.02147	0.40697	0.00114	0.14378	3.65702E-4
14	9.99997	0.02464	0.39146	7.4619E-4	0.14315	7.53572E-4
15	10.49998	0.0365	0.37052	5.96374E-4	0.0966	0.00111
16	11.00026	0.03264	0.35987	4.70226E-4	0.11769	0.00121
17	11.49997	0.03798	0.34925	3.807E-4	0.12784	3.70892E-4
18	11.99982	0.03921	0.3369	2.97893E-4	0.13334	3.04063E-4
19	12.49982	0.03196	0.32439	2.18515E-4	0.15862	2.20861E-4
20	12.99994	0.05613	0.31143	1.92221E-4	0.12048	6.46527E-4

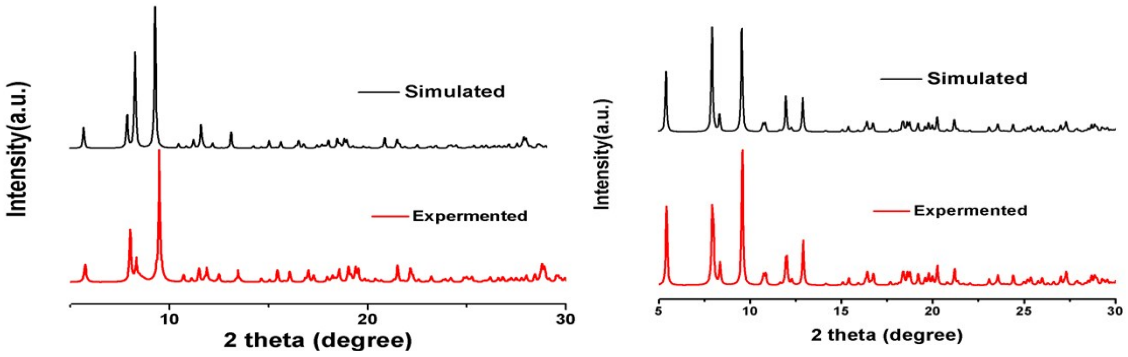

Figure S1. PXRD patterns and simulated patterns generated from single crystal diffraction data for compounds **1** (left) and **1'** (right).

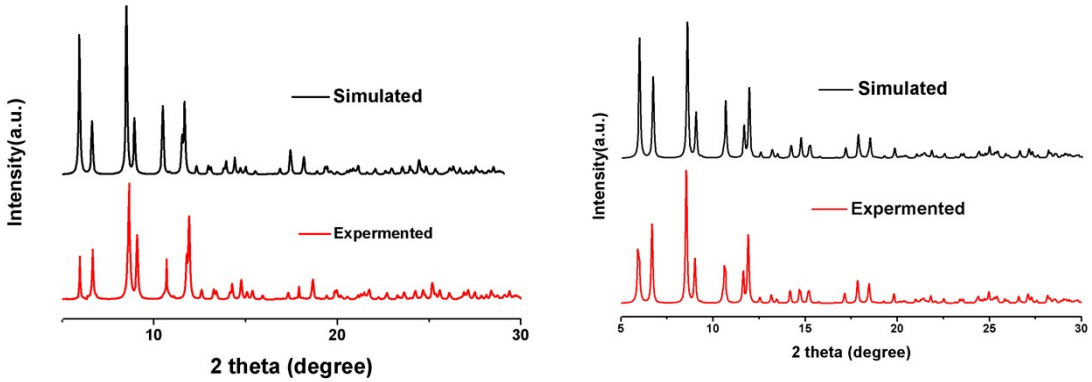

Figure S2. PXRD patterns and simulated patterns generated from single crystal diffraction data for compounds **2** (left) and **2'** (right).

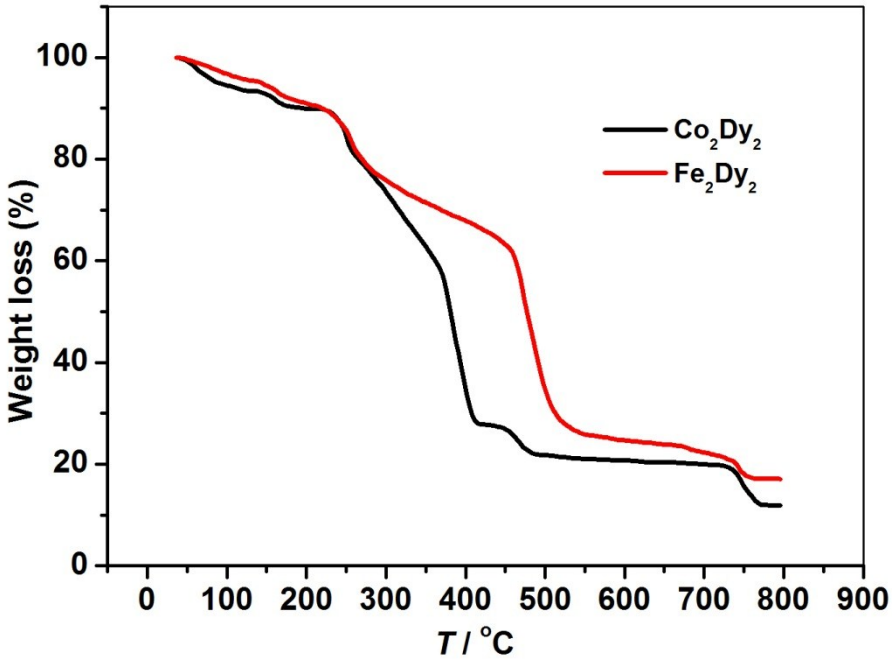

Figure S3. Plots of TGA for complexes **1** and **2**.

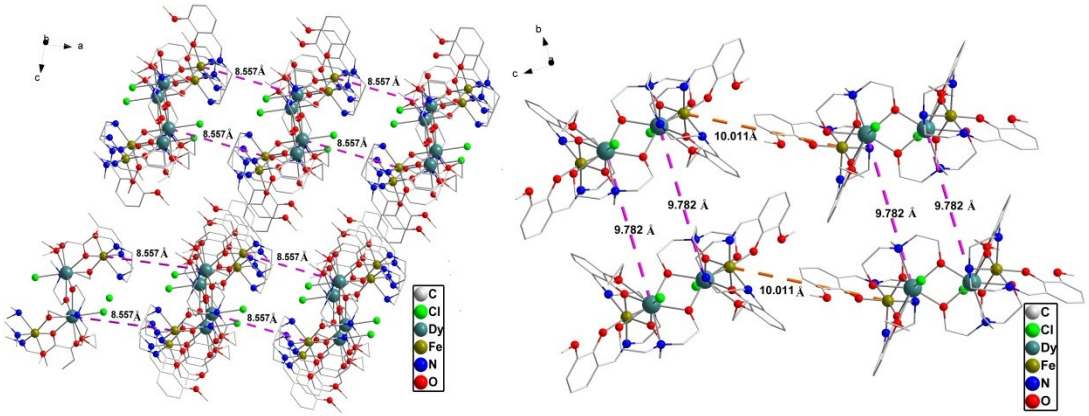

Figure S4. The plots show the shortest distances of $Fe^{III}\cdots Dy^{III}$ (left), $Dy^{III}\cdots Dy^{III}$ and $Fe^{III}\cdots Fe^{III}$ (right) between the nearest neighbor molecules of **1**. For clarity, the H atoms and solvent molecules were omitted.

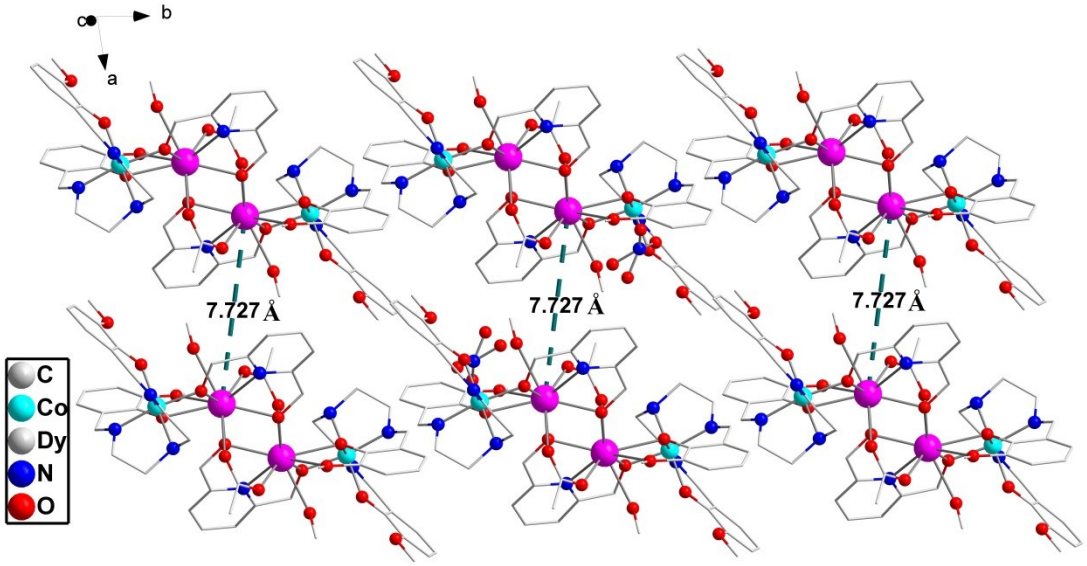

Figure S5. The plots show the shortest distances of $Dy^{III}\cdots Dy^{III}$ between the nearest neighbor molecules of **2**. For clarity, the H atoms and solvent molecules were omitted.

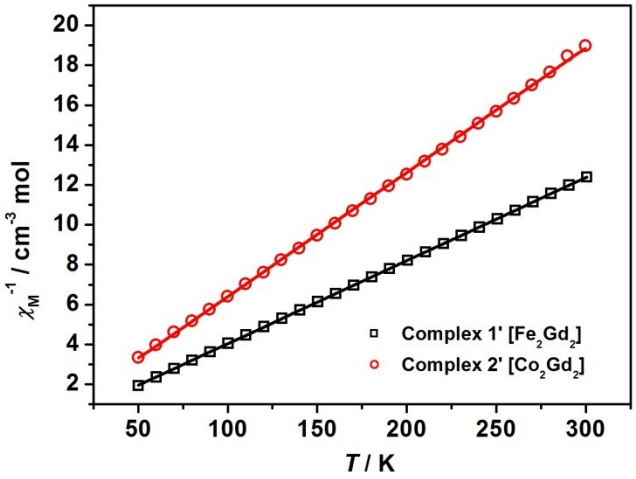

Figure S6. Plots of χ_M^{-1} *vs T* for complexes **1'** and **2'**; the black and red solid lines represent the fitted results by the Curie-Weiss law.

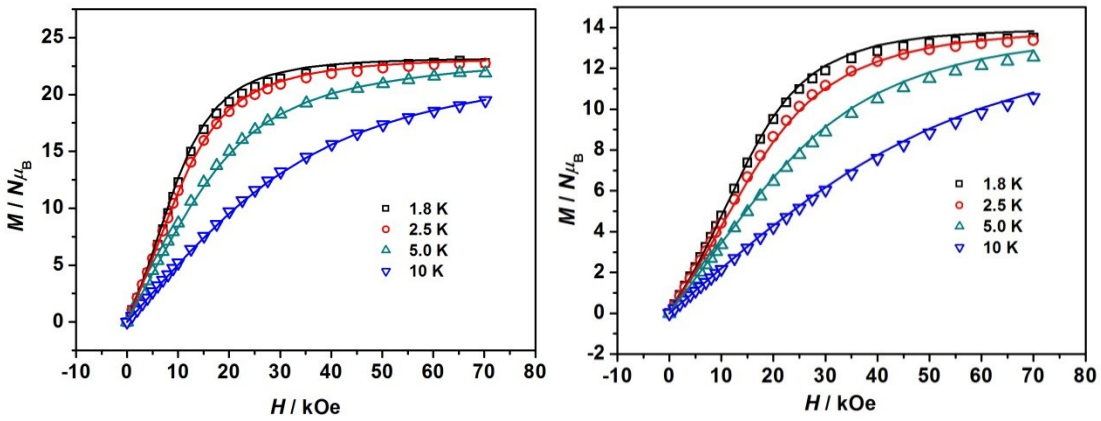

Figure S7. *M vs H* plots for complexes **1'** ([Fe_2Gd_2], left) and **2'** ([Co_2Gd_2], right); the solid lines represent the fitted results by PHI program.

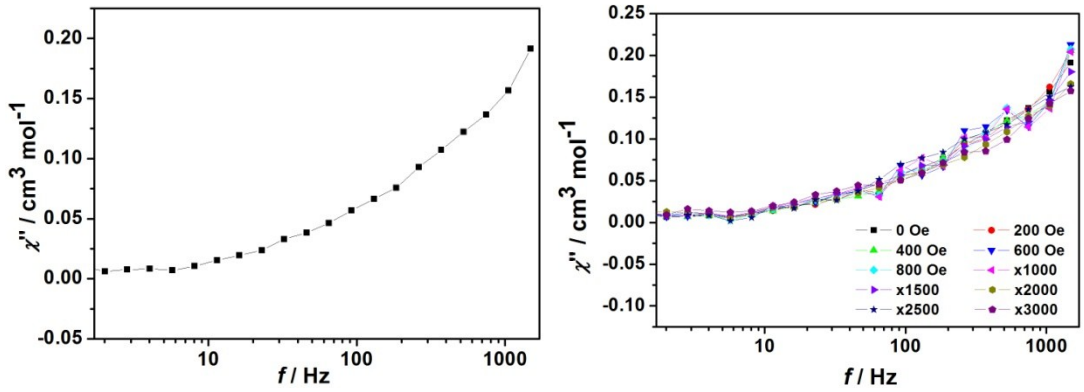

Figure S8. (Left) Plots of out-of-phase (χ_M'') versus *f* (left) for **1** at 2.0 K under zero dc field at various frequencies from 1 to 1488 Hz. **Notably,** the single curve clearly indicates that for complex **1**, χ_M'' signals were observed, but no peaks were found. Therefore, ac susceptibility measurements for **1** under zero dc fields at other temperatures were not performed. (Right) Out-of-phase (χ_M'') versus *f* for complex **1** at 2.0 K under the dc fields from 0 Oe to 3000 Oe and with the frequencies from 1 to 1488 Hz.

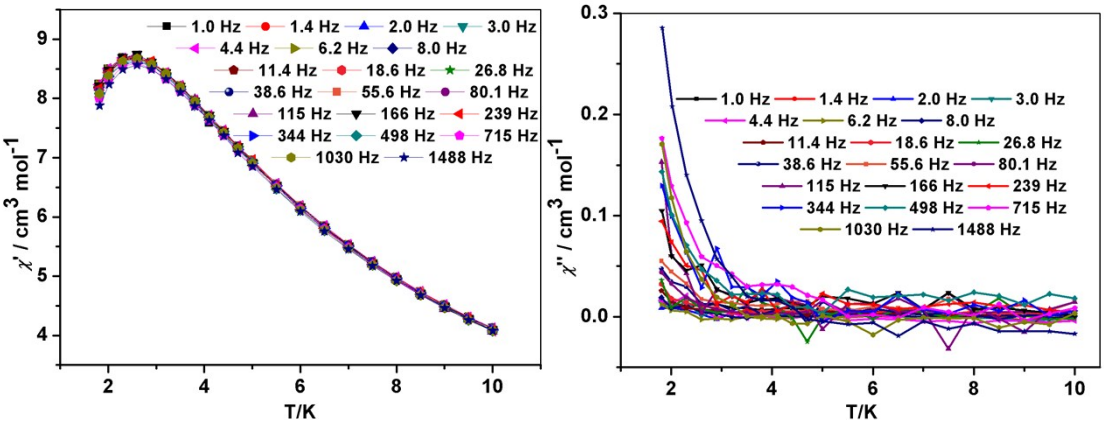

Figure S9. Plots of in-phase (χ_M') versus *T* (left) and out-of-phase (χ_M'') versus *T* (right) for complex **1** at 1000 Oe dc field.

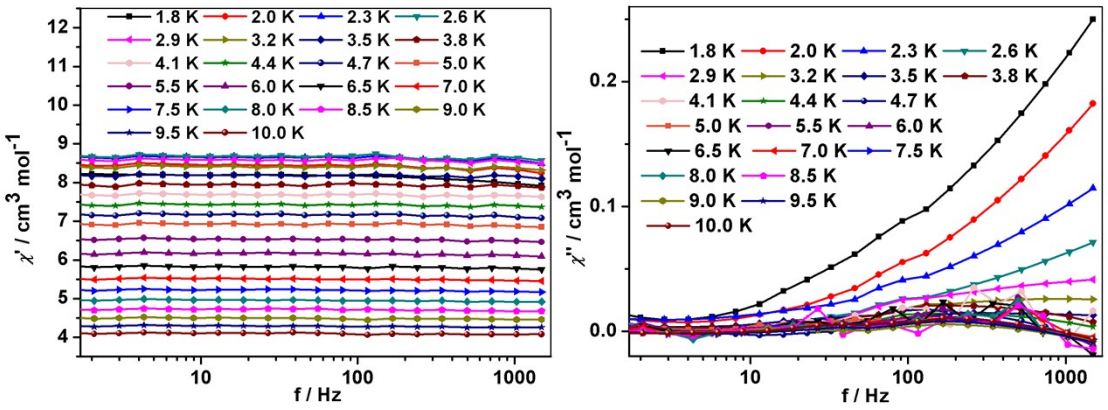

Figure S10. Plots of in-phase (χ_M') versus f (left) and out-of-phase (χ_M'') versus f (right) for **1** at 1000 Oe dc field.

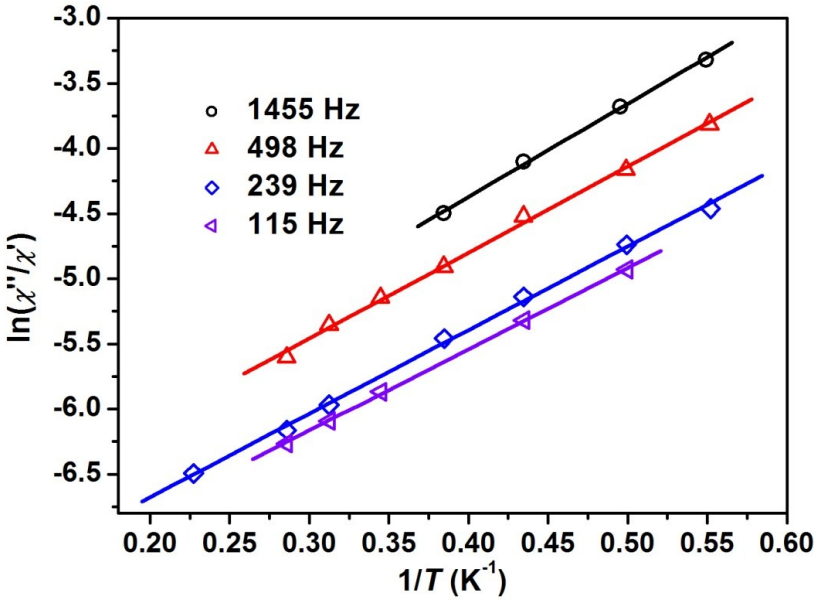

Figure S11. Plots of ln(χ''/χ') *versus* 1/T at different frequencies for complex **1**.

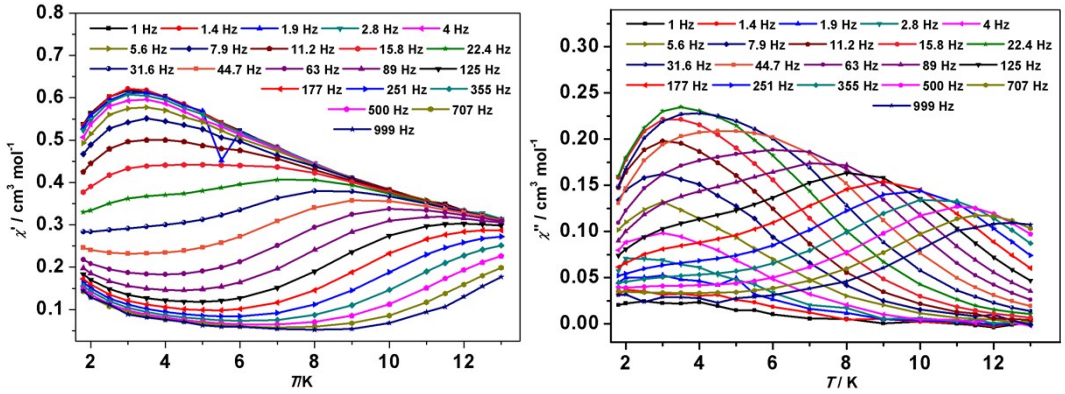

Figure S12. Plots of in-phase (χ_M') versus T (left) and out-of-phase (χ_M'') versus T (right) for complex **2** at 0 Oe dc field.

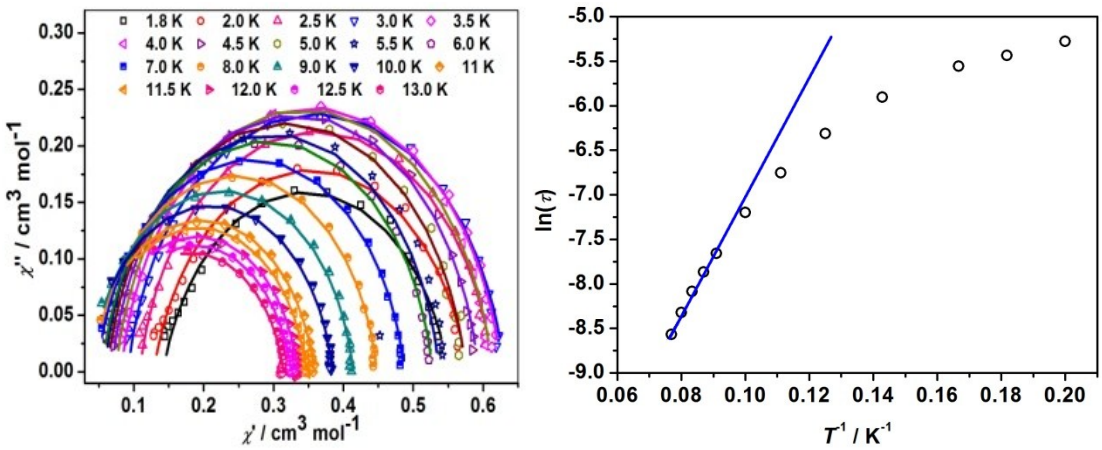

Figure. S13 Cole-Cole plots for complex **2** under 0 Oe dc field (left). Solid lines show the fit of the data by employing the generalized single relaxation process Debye model. Arrhenius plots of ln(τ) vs T^{-1} under 0 Oe for complex **2** (right). The blue lines show the fit of the data to the Arrhenius law $\tau = \tau_0 \exp(U_{eff}/kT)$, assuming the Orbach relaxation process.

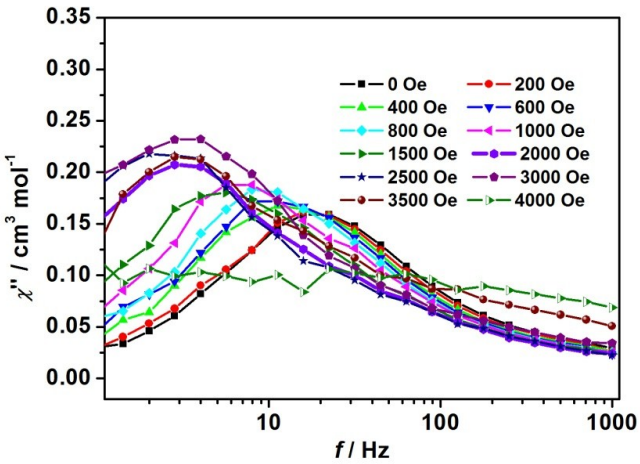

Figure S14. Plots of out-of-phase (χ_M'') versus f for complex **2** at 1.8 K under the dc fields from 0 Oe to 4000 Oe and with the frequencies from 1 to 999 Hz. To see easily, the optimal dc field employed by us were represented by thick violet line.

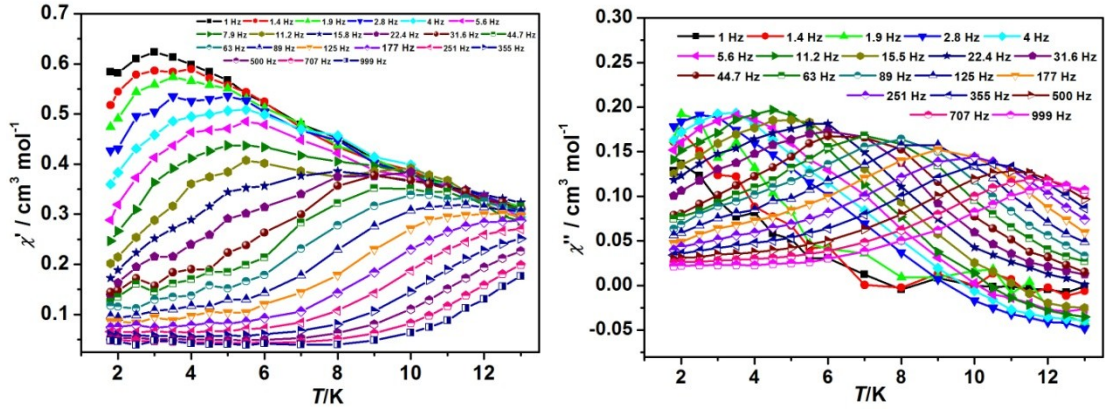

Figure S15. Plots of in-phase (χ_M', left) and out-of-phase (χ_M'', right) versus T for complex **2** at 1.8-13 K under 2000 Oe dc field with the frequency ranging from 1 to 999 Hz.

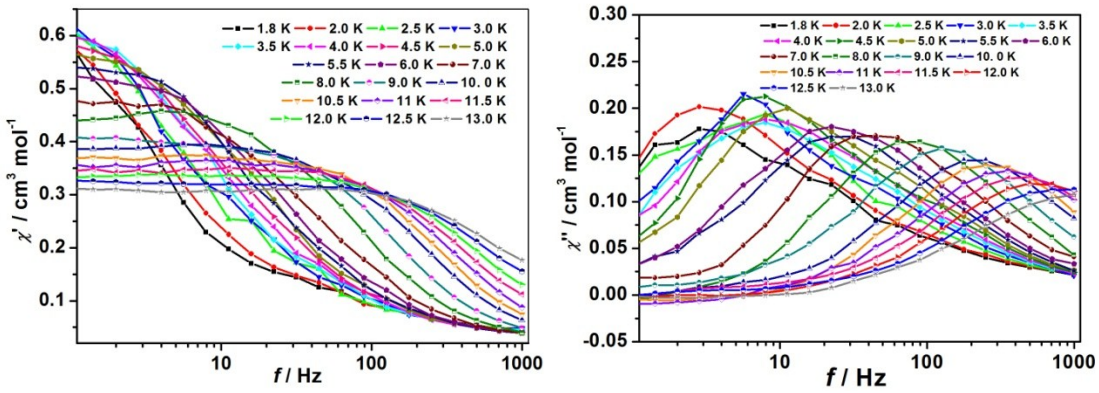

Figure S16. Plots of in-phase (χ_M', left) and out-of-phase (χ_M'', right) versus *f* for complex **2** at 1.8-13 K under 2000 Oe dc field with the frequency ranging from 1 to 999 Hz.

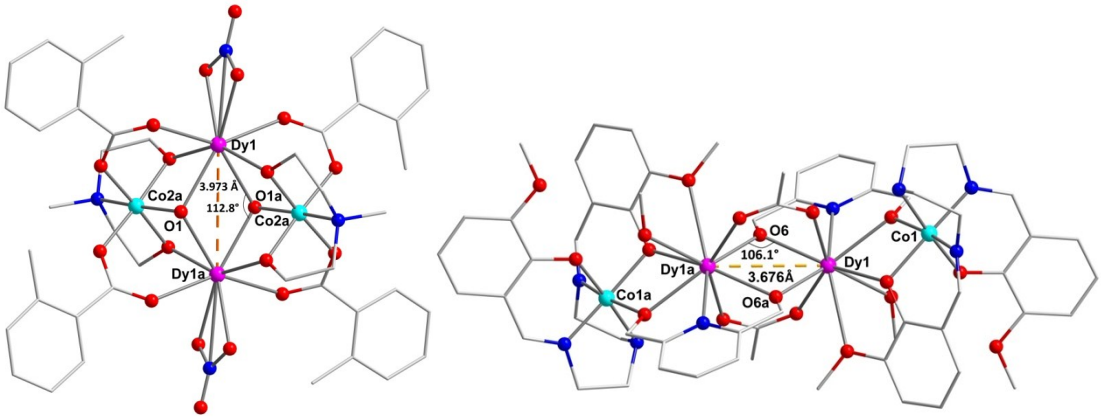

Figure S17. The plots showing the distances of $Dy^{III}\cdots Dy^{III}$ and angles of Dy1O1Dy1a (or Dy1O6Dy1a, bottom) for the complex reported by others (top) and the complex **2** reported in this work (bottom). Symmetry codes, a 1-x, 2-y, 2-z (top); a –x, 1-y, 1-z (bottom).

Computational details

For **1**, two Dy^{III} and Fe^{III} fragments will be calculated. For compound **2**, only one type of Dy^{III} fragment needs to be calculated due to its symmetry. Complete-active-space self-consistent field (CASSCF) calculations on individual Dy^{III} or Fe^{III} fragments indicated as **1_Dy**, **1_Fe** and **2_Dy** (see Figure S18 for the calculated structures of complexes **1** and **2**) on the basis of single-crystal X-ray determined geometry have been carried out with MOLCAS 8.2 program package. Each individual Dy^{III} or Fe^{III} fragment in **1** and **2** was calculated keeping the experimentally determined structure of the corresponding compound while the neighboring Dy^{III}, Co^{III} (or Fe^{III}) ions were replaced by diamagnetic Lu^{III} and Sc^{III}, respectively.

The basis sets for all atoms are atomic natural orbitals from the MOLCAS ANO-RCC library: ANO-RCC-VTZP for Dy^{III} or Fe^{III}; VTZ for close N and O; VDZ for distant atoms. The calculations employed the second order Douglas-Kroll-Hess Hamiltonian, where scalar relativistic contractions were taken into account in the basis set and the spin-orbit couplings were handled separately in the restricted active space state interaction (RASSI-SO) procedure. For individual Dy^{III} fragment, active electrons in 7 active spaces include all *f* electrons (CAS(9 in 7)), active electrons in 5 active spaces include all *d* electrons (CAS(5 in 5)) for Fe^{III} fragment in the CASSCF calculation. To exclude all the doubts, we calculated all the roots in the active space. We have mixed the maximum number of spin-free state which was possible with our hardware (all from 21 sextets, 128 from 224 quadruplets, 130 from 490 doublets). SINGLE_ANISO program was used to obtain the energy levels, $\boldsymbol{g}$ tensors, m_J values, magnetic axes, *et al.,* based on the above CASSCF/RASSI-SO calculations.

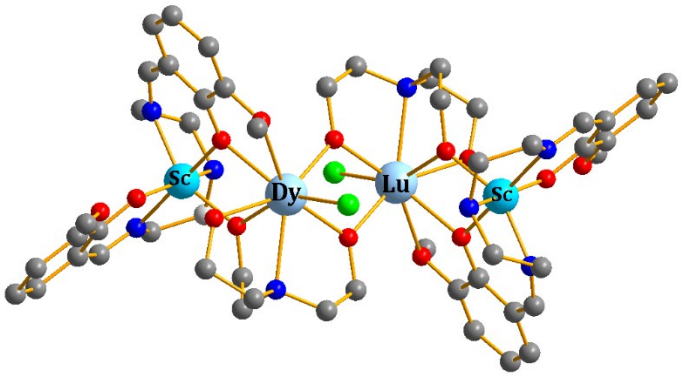

1_Dy

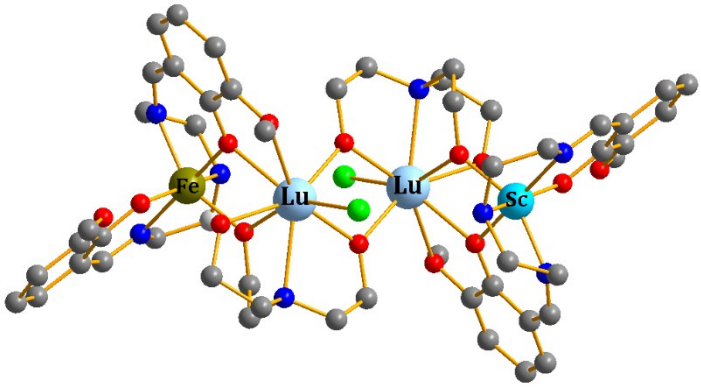

1_Fe

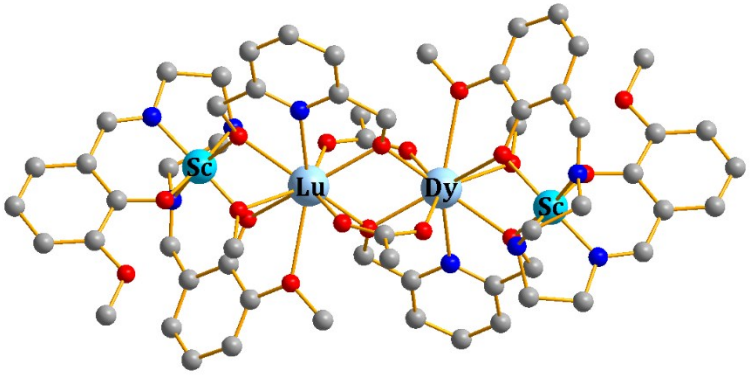

2_Dy

Figure S18. Calculated model structures of **1_Dy**, **1_Fe** and **2_Dy**; H atoms are omitted.

Table S11. Calculated energy levels (cm^{-1}), ***g*** (g_x, g_y, g_z) tensors and predominant m_J values of the lowest eight Kramers doublets (KDs) of **1_Dy** and **2_Dy**, and zero-field splitting parameters D (E) (cm^{-1}), ***g*** (g_x, g_y, g_z) tensor of the lowest spin-orbit state of **2_Fe** using CASSCF/RASSI-SO with MOLCAS 8.2.

KDs	**1_Dy**			**1_Fe**		**2_Dy**		
	E/cm^{-1}	***g***	m_J	D(E)	***g***	E/cm^{-1}	***g***	m_J
1	0.0	0.286 0.511 19.086	±15/2	0.12(-0.03)	2.002 2.002 2.002	0.0	0.012 0.020 19.742	±15/2
2	28.4	0.332 1.129 17.871	±3/2			146.4	0.109 0.181 17.874	±13/2
3	68.5	0.209 1.377 16.294	±11/2			227.4	0.724 1.498 13.719	±11/2
4	142.8	0.975 1.532 15.695	±13/2			267.1	1.812 4.832 14.089	±1/2
5	157.6	0.422 3.482 11.016	±7/2			318.4	8.959 6.823 0.218	±5/2

6	222.0	4.339 5.436 8.347	±5/2		353.8	2.457 4.652 14.017	±3/2
7	317.1	1.567 2.210 12.089	±1/2		466.3	0.459 1.721 13.770	±7/2
8	356.3	0.824 4.657 15.318	±9/2		499.4	0.281 2.229 15.517	±9/2

Table S12. Wave functions with definite projection of the total moment | m_J > for the lowest two KDs of individual Dy^{III} fragments for **1_Dy** and **2_Dy** using CASSCF/RASSI-SO with MOLCAS 8.2.

	E/cm^{-1}	wave functions
1_Dy	0.0	91.54%|±15/2>
	28.4	19.49%|±7/2>+26.75%|±5/2>+18.79%|±3/2>+15.47%|±1/2>+7.43%|±11/2>
2_Dy	0.0	98.67%|±15/2>
	146.4	62.63%|±13/2>+21.48%|±11/2>+8.93%|±9/2>

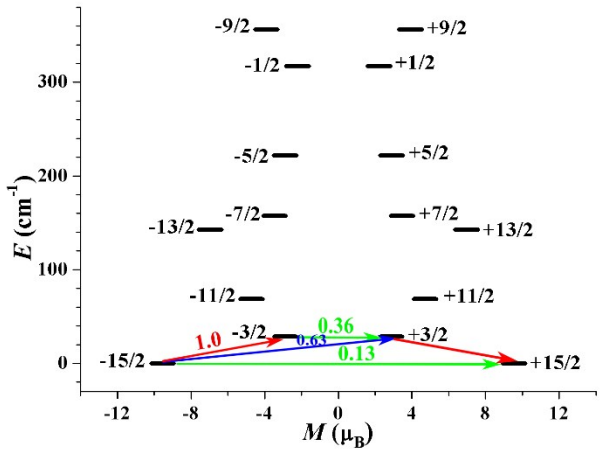

1_Dy

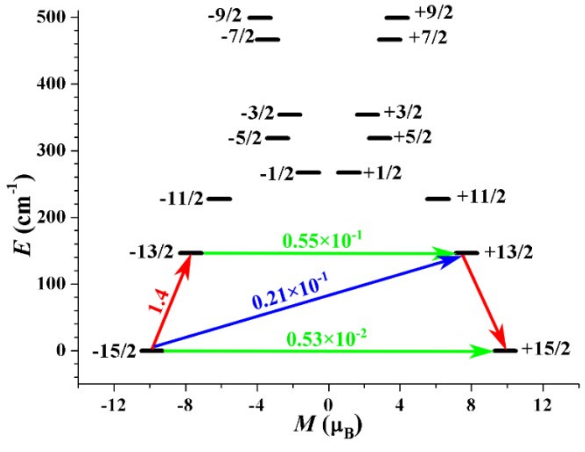

2_Dy

Figure S19. Magnetization blocking barriers for individual Dy^{III} fragments of **1_Dy** and **2_Dy**. The thick black lines represent the KDs of the individual Dy^{III} fragments as a function of their magnetic moment along the magnetic axis. The green lines correspond to diagonal matrix element of the transversal magnetic moment; the blue line represent Orbach relaxation processes. The path shown by the red arrows represents the most probable path for magnetic relaxation in the corresponding compounds. The numbers at each arrow stand for the mean absolute value of the corresponding matrix element of transition magnetic moment.

To fit the exchange interactions in complexes **1** and **2**, we took two steps to obtain them. Firstly, we calculated individual Dy^{III} or Fe^{III} fragments using CASSCF/RASSI-SO to obtain the corresponding magnetic properties. Then, the exchange interaction between the magnetic centers is considered within the Lines model, while the account of the dipole-dipole magnetic coupling is treated exactly. The Lines model is effective and has been successfully used widely in the research field of *d* and *f*-elements single-molecule magnets.

For compounds **1** and **2**, there are two and one types of ,respectively.

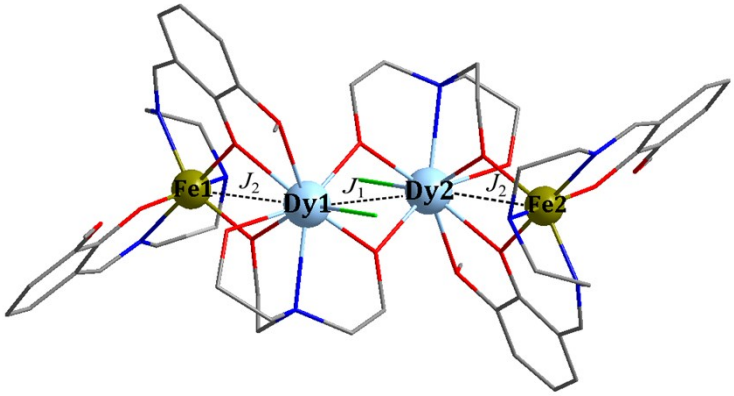

1

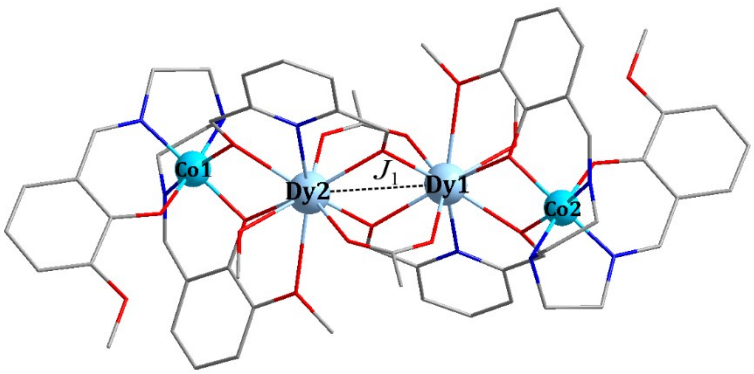

2

Figure S20. Two types of J_1 and J_2 in **1** and one type of J_1 in **2**.

The Ising exchange Hamiltonians for **1** and **2** are:

$$\hat{H}_{exch} = -J_1 \hat{S}_{Dy1} \hat{S}_{Dy2} - J_2 \hat{S}_{Dy1} \hat{S}_{Fe1} - J_2 \hat{S}_{Dy2} \hat{S}_{Fe2} \quad \text{for } \mathbf{1} \qquad (1)$$

$$\hat{H}_{exch} = -J_1 \hat{S}_{Dy1} \hat{S}_{Dy2} \quad \text{for } \mathbf{2} \qquad (2)$$

The J_1 and J_2 are the effective exchange coupling constants between Dy1-Dy2 and Dy1-Fe1 (Dy2-Fe2), respectively. The $S_{Dy} = 1/2$ is the ground pseudospin on the Dy^{III} sites and the $S_{Fe} = 5/2$ is the ground spin on the Fe^{III} ions. The dipolar magnetic coupling can be calculated exactly, while the exchange coupling constants were fitted through comparison of the computed and measured magnetic susceptibility using the POLY_ANISO program.

Table S13. Exchange energies E (cm^{-1}), the energy difference between each exchange doublets Δ_t (cm^{-1}) and the main values of the g_z for the lowest eight and two exchange doublets of **1** and **2**.

	1			**2**		
	E	Δ_t	g_z	E	Δ_t	g_z
1	0.0	3.6×10^{-4}	0.000	0.0	3.6×10^{-6}	0.000
2	1.1	3.5×10^{-4}	51.007	2.5	2.6×10^{-6}	39.481
3	4.1	9.4×10^{-4}	0.000			
4	4.1	7.2×10^{-4}	0.000			
5	5.1	1.4×10^{-3}	38.148			
6	5.1	3.0×10^{-3}	38.152			
7	8.3	1.7×10^{-3}	0.000			
8	9.2	1.7×10^{-3}	30.760			

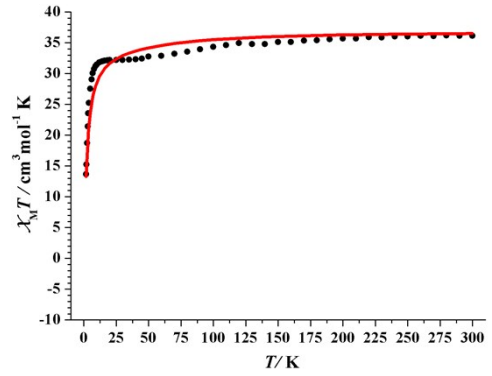

1

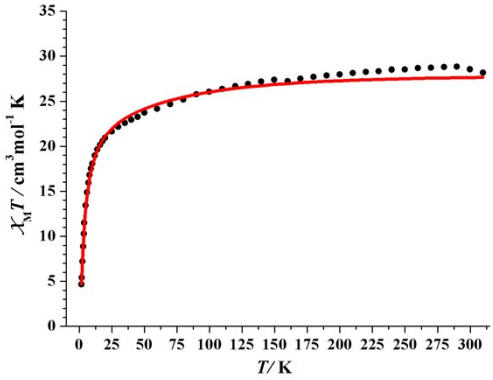

2

Figure S21. Calculated (red solid line) and experimental (black dot) data of magnetic susceptibilities of **1** and **2**. The intermolecular interactions zJ' of **1** and **2** were fitted to −0.10 and −0.09 cm^{-1}, respectively.

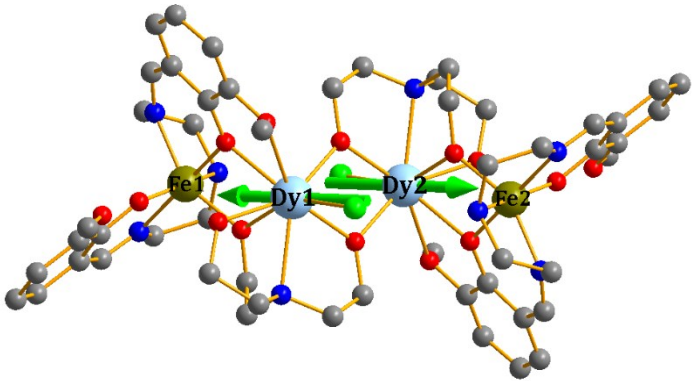

1

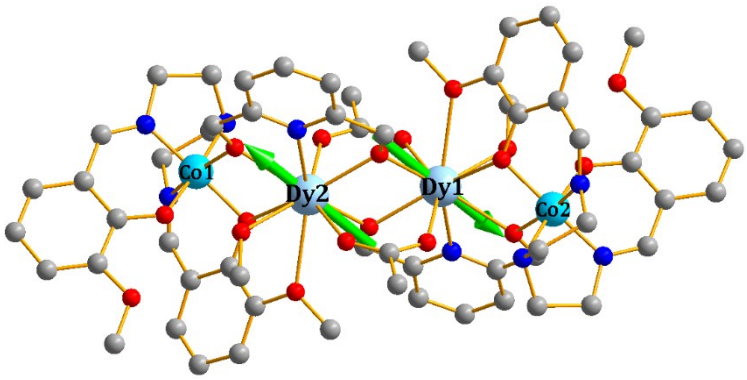

2

Figure S22. Calculated orientations of the local main magnetic axes in the ground KDs on Dy^{III} ions of complexes **1** and **2**.

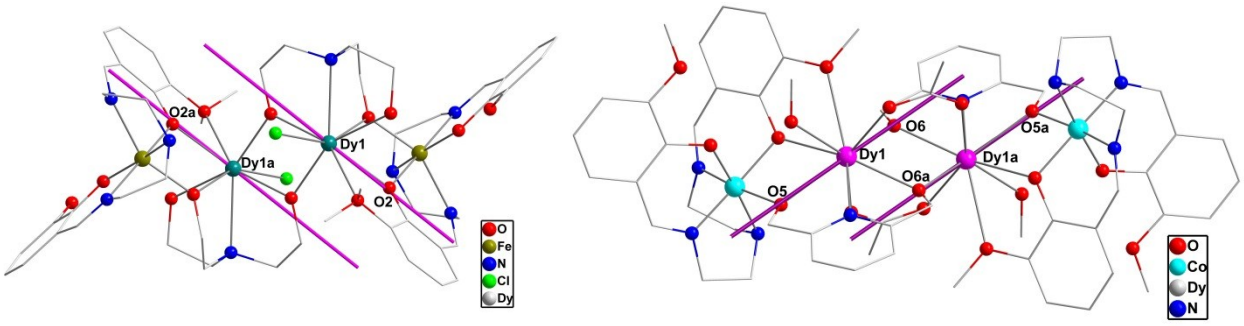

Figure S23. Ground-state magnetic anisotropy of **1** (left) and **2** (right) calculated by Magellan Software. The thick line represents the orientation of the anisotropy axis for two Dy^{III} ions in both complexes.